Laser and Particle Beams (2013), *31*, 663–671.

doi:10.1017/S0263034613000700

Laser irradiation of thin films: Effect of energy transformation

MIKHAIL E. POVARNITSYN,[1] NIKOLAY E. ANDREEV,[1] PAVEL R. LEVASHOV,[1] KONSTANTIN V. KHISHCHENKO,[1] DMITRY A. KIM,[2] VLADIMIR G. NOVIKOV,[2] AND OLGA N. ROSMEJ[3]

[1]Joint Institute for High Temperatures RAS, Moscow, Russia and Moscow Institute of Physics and Technology (State University), Dolgoprudny, Moscow Region, Russia
[2]Keldysh Institute of Applied Mathematics, Moscow, Russia
[3]GSI Helmholtzzentrum für Schwerionenforschung GmbH, Darmstadt, Germany

(Received 30 May 2013; Accepted 11 July 2013)

Abstract

The irradiation of thin films by intensive subpicosecond laser pulses with nanosecond prepulse is accompanied by a number of various physical processes. The laser beam transmissions through the film as well as the re-emission flux on both sides of the film plasma have been evaluated by simulation for Al and CH_2 materials. It has been demonstrated that the thickness of the film can be chosen to cut off the long nanosecond prepulse whereas the main pulse is transmitted through the plasma. Thus, thin films can be useful for the laser contrast improvement in experiments with different targets.

Nevertheless, the laser energy transformation into the soft X-ray radiation on the back side of the shielding film plasma can reach up to 7% of the incident intensity for the Al film and result in strong preheating of the target. At the same time the re-emission flux produced by a CH_2 film is an order lower than that in the case of Al film. The shielding of an Ag bulk target by Al and CH_2 films is simulated and discussed.

Keywords: High-intensity lasers; Laser contrast; Nanosecond prepulse; Two-temperature hydrodynamics; Re-emission flux

INTRODUCTION

The irradiation of different materials by subpicosecond laser pulses with relativistic intensities $I \gtrsim 10^{19}$ W/cm^2 is widely used (Ditmire *et al*., 2004), especially for the development of X-ray sources, warm dense matter investigation (Zastrau *et al*., 2010), fast ignition (Kitagawa *et al*., 2004), radiative shocks (Stehlé *et al*., 2010), and particle acceleration (Carroll *et al.*, 2010). For these experiments, the laser contrast is a key parameter that can be defined as the ratio of the prepulse intensity to the peak one. Depending on the pulse amplification technique, the duration and intensity of the prepulse can vary, and the contrast ratio in the case of chirped amplification at ~1 ns before the main short pulse is about 10^{-6} as reported (Bagnoud *et al*., 2010). Undesirable effects of the long prepulse can be reduced at least several orders of magnitude using the plasma mirror technique (Carroll *et al*., 2010; Doumy *et al*., 2004) or frequency doubling (Zastrau *et al*., 2010). Actual laser setups with good enough characteristics produce a contrast of the order of 10^{-8} that gives the intensity level $I \sim 10^{12}$ W/cm^2 for the nanosecond prepulse. Such prepulse intensity is sufficient to produce plasma at the surface of a solid target, change the dynamics of high-intensity laser-matter interaction (McKenna *et al.*, 2006), and destroy the surface-structured targets (Ovchinnikov *et al.*, 2011).

In our recent paper (Povarnisyn *et al*., 2012*a*), we discussed the possible way of the contrast improvement by placing a thin metal film ahead of the main target and thereby cutting off the long nanosecond prepulse. The multi-stage thin film dynamics has been investigated from the initial stage of the film heating, material rarefaction until the moment of almost full ionization and electron density dropping below the critical value when the plasma becomes transparent for the laser beam. Another important process that determines the channel of laser energy transformation is the re-emission effect that governs both the radiation heating of the film and emissivity of the film plasma. The later case,

Address correspondence and reprint requests to: Mikhail E. Povarnitsyn, Joint Institute for High Temperatures RAS, Izhorskaya 13 Bldg 2, Moscow 125412, Russia. E-mail: povar@ihed.ras.ru

as was shown earlier (Povarnistyn *et al*., 2012*a*), is important for proper estimation of the main target preheating.

In this paper, we analyze numerically the dynamics of thin films irradiated by a nanosecond prepulse using the wide-range model of radiation hydrodynamics (Povarnitsyn *et al.*, 2012*a*). The paper is organized as follow. The first section introduces baseline designs. In the second section, we describe the basic features of the model. Then, the third section is devoted to results of modeling for Al and CH_2 films and Ag target.

MODEL

Equations of Radiation Hydrodynamics

The basic features of the model used for simulation of the laser-matter interaction are described (Povarnitsyn *et al.*, 2012*a*). The model takes account of 1D hydrodynamic motion of substance, laser energy absorption, two-temperature nonequilibrium states for electron and ion subsystems, electron thermal conductivity and radiation transport in diffusion approximation. The evolution of material parameters is described using the conservation of mass, momentum and energy of electron and ion subsystems in a single-fluid two-temperature Lagrangian form:

$$\frac{\partial(1/\rho)}{\partial t} - \frac{\partial u}{\partial m} = 0, \tag{1}$$

$$\frac{\partial u}{\partial t} + \frac{\partial(P_i + P_e)}{\partial m} = 0, \tag{2}$$

$$\frac{\partial e_e}{\partial t} + P_e \frac{\partial u}{\partial m} = -\gamma_{ei}(T_e - T_i)/\rho + Q_L/\rho + \frac{\partial}{\partial m}\left(\rho\kappa_e \frac{\partial T_e}{\partial m}\right) - \frac{\partial S}{\partial m}, \tag{3}$$

$$\frac{\partial e_i}{\partial t} + P_i \frac{\partial u}{\partial m} = \gamma_{ei}(T_e - T_i)/\rho. \tag{4}$$

Here ρ is the density; t is the time; m is the mass coordinate, $dm = \rho dz$ with the space coordinate z; u is the velocity; P, e, T are the pressure, specific energy and temperature, respectively. Indices e and i stand for electron and ion species. The energy exchange between electrons and ions is described by the corresponding term with the coupling factor $\gamma_{ei}(\rho, T_e, T_i)$. The electron heat transfer is specified with the aid of the thermal conduction coefficient $\kappa_e(\rho, T_e, T_i)$. Optical and transport properties of Al and Ag plasma are taken into account by means of wide-range models (Povarnisyn *et al*., 2012b; Veysman *et al*., 2008). For CH_2 material, we use a similar approach interpolating between dense preionized state (Drude model) and Spitzer ideal plasma (Spitzer & Härm, 1953). The key parameter in these models is the frequency of collisions (electron–phonon, electron–ion, and electron–electron). In the metal state, it can be written as follows

$$\nu_{\text{met}} = A_1 k_B T_i/\hbar + A_2 k_B T_e^2/(T_F\hbar). \tag{5}$$

Here k_B and $\hbar$ are the Boltzmann and Planck constants, respectively, and T_F is the Fermi temperature. The frequency is limited from above by the electron free-path between ions so that

$$\nu_{\max} = \frac{A_3}{r_0}\sqrt{v_F^2 + k_B T_e/m_e}, \tag{6}$$

where v_F is the Fermi speed of electrons, r_0 is the interatomic distance and m_e is the electron mass.

For hot states $T_e \gg T_F$ with not very high densities, the plasma model (Spitzer & Härm, 1953) is relevant

$$\nu_{\text{pl}} = \frac{4}{3}\sqrt{2\pi}\frac{\langle Z\rangle n_e e^4 \Lambda}{\sqrt{m_e}(k_B T_e)^{3/2}}, \tag{7}$$

where $\langle Z\rangle$ is the mean charge of ions, n_e is the electron concentration, e is the electron charge, and Λ is the Coulomb logarithm.

The electron thermal conductivity in the metal is calculated according to the Drude formalism as follows

$$\kappa_{\text{met}} = \frac{\pi^2 k_B^2 n_e}{3 m_e \nu_{\text{eff}}} T_e, \tag{8}$$

where $\nu_{\text{eff}} = \min(\nu_{\text{met}}, \nu_{\max})$. The hot plasma limit is

$$\kappa_{\text{pl}} = \frac{16\sqrt{2}\, k_B (k_B T_e)^{5/2}}{\pi^{3/2}\langle Z\rangle e^4 \sqrt{m_e}\Lambda}. \tag{9}$$

An interpolation between (8) and (9) in the vicinity of the Fermi temperature gives us a wide-range expression for the thermal diffusivity,

$$\kappa = \kappa_{\text{pl}} + (\kappa_{\text{met}} - \kappa_{\text{pl}})\exp[-A_4 T_e/T_F]. \tag{10}$$

The dimensionless parameters A_1, A_2, A_3, A_4 are used to adjust the model to available theoretical and experimental data. For the thermal conduction of Ag, the parameters are ${A_1}^t = 0.7, A_2^t = 0.5, A_3^t = 1.0, A_4^t = 3.0$. In Figure 1, we compare the results of the interpolation (10) with the theoretical data (Apfelbaum, 2011) for normal and 0.1 of normal density. Appropriate coefficients of the model for Al are $A_1^t = 2.95, A_2^t = 0.5, A_3^t = 0.16, A_4^t = 1.2$, see Figure 2 in paper by-Povarnitsyn *et al*. (2012*b*).

The coupling factor is written in the form

$$\gamma_{ei} = \frac{3 k_B m_e}{m_i} n_e \nu_{\text{eff}}, \tag{11}$$

https://doi.org/10.1017/S0263034613000700 Published online by Cambridge University Press

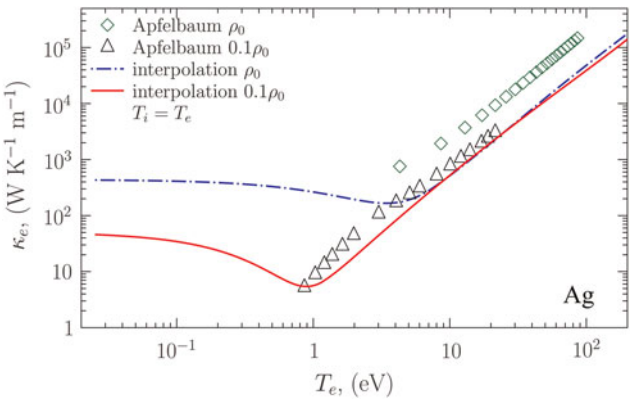

Fig. 1. (Color online) The thermal conductivity coefficient of Ag. Comparison of interpolation formula (10) (lines) with available theoretical data (Apfelbaum, 2011) (signs) in cases of normal and 0.1 of normal densities, $T_i = T_e$.

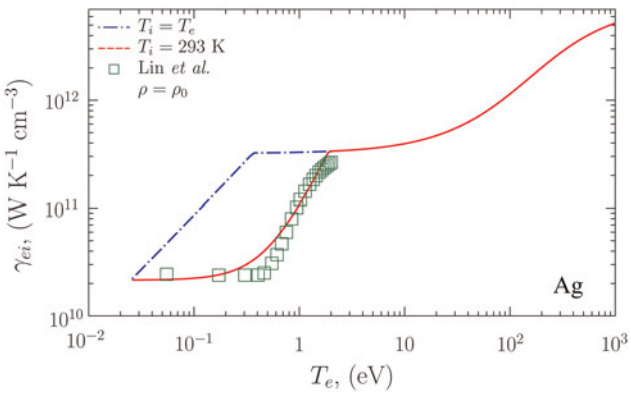

Fig. 2. (Color online) The coupling factor of Ag according to the model (11) (lines) and theoretical results (Lin *et al.*, 2008) (signs) for normal density.

where m_i is the ion mass, and $\nu_{\text{eff}} = \min(\nu_{\text{met}}, \nu_{\max}, \nu_{\text{pl}})$ is given by expressions (5), (6), (7). For Ag, the dimensionless parameters are $A_1^g = 10.0$, $A_2^g = 10.0$, $A_3^g = 0.4$. The coupling factor (11) and results of first-principle calculations (Lin *et al.*, 2008) are presented in Figure 2 for Ag. Appropriate coefficients for Al can be found in paper by Povarnitsyn *et al.* (2012*b*).

The laser energy absorption (bremsstrahlung process) is taken into account with the aid of heat source term Q_L (t, z). To find it we solve the Helmholtz wave equation for the laser electric field with proper boundary conditions (Povarnitsyn *et al.*, 2012*a*)

$$\frac{\partial^2 E}{\partial z^2} + \frac{\omega_L^2}{c^2}\epsilon(z)E = 0.$$

Here the normal incidence is supposed, E is the laser electric field envelope, ω_L is the laser frequency, c is the speed of light, $\epsilon(\rho, T_e, T_i)$ is the complex dielectric function. The resulting laser heating source is

$$Q_L(t, z) = I(t)\frac{\omega_L}{c}\text{Im}\{\epsilon(t, z)\}|E(t, z)/E_L(t)|^2,$$

where the incident laser field amplitude is $E_L(t) = \sqrt{8\pi I(t)/c}$.

The radiation transport is taken into account by the integral over the spectrum flux $S = \int_\omega S_\omega d\omega$. The equations of radiation transport are written in diffusion approximation:

$$\frac{\partial S_\omega}{\partial z} = 4\pi j_\omega - \kappa_\omega c U_\omega, \tag{12}$$

$$S_\omega = -\frac{c}{3\kappa_\omega}\frac{\partial U_\omega}{\partial z}, \tag{13}$$

$$S_\omega|_\Omega = \mp\frac{cU_\omega}{2}, \tag{14}$$

where S_ω is the radiation flux density, U_ω is the radiant energy density, j_ω and κ_ω are the coefficients of emissivity and absorption, respectively, and Ω is the external boundary of plasma.

Equations of state (EOSs) for Al, CH_2, and Ag determine the relations $P_e(\rho, T_e)$, $P_i(\rho, T_i)$, $e_e(\rho, T_e)$, $e_i(\rho, T_i)$ and are necessary for completeness of system (1)–(4). These EOSs are based on the analytical expression of the Helmholtz free energy that has a form $\mathcal{F}(\rho, T_i, T_e) = \mathcal{F}_i(\rho, T_i) + \mathcal{F}_e(\rho, T_e)$, and is composed of two parts. The first item stands for the ionic part $\mathcal{F}_i(\rho, T_i) = \mathcal{F}_c(\rho) + \mathcal{F}_a(\rho, T_i)$, and consists of the electron-ion interaction term $\mathcal{F}_c$ (calculated at $T_i = T_e = 0$ K) and the contribution of the thermal motion of ions $\mathcal{F}_a$. The analytical form of $\mathcal{F}_i$ has different expressions for solid and fluid phases (Khishchenko, 2008). The tables of thermodynamic parameters are calculated to take into account phase transitions and metastable regions (Khishchenko *et al.*, 2002; Levashov & Khishchenko, 2007; Oreshkin *et al.*, 2004). The second term $\mathcal{F}_e(\rho, T_e)$ describes the thermal contribution of electrons calculated with the aid of the Thomas–Fermi model (Shemyakin *et al.*, 2010).

Absorption and Emission Coefficients

As was demonstrated in Povarnitsyn *et al.* (2012*a*) the radiation transport is a key effect in the dynamics of thin films illuminated by nanosecond prepulses with intensity $\gtrsim 10^{11}$ W/cm^2. Transformation of monochromatic laser energy into a wide spectrum of photons results in formation of noticeable re-emission fluxes on both sides of the film. We focus here on the detailed description of the procedure for calculation of absorption and emission coefficients. These coefficients depend on ion concentrations. To obtain concentrations x_{ks} of k-fold ionized atoms or molecules in the state s the system of level kinetic equations is solved in

https://doi.org/10.1017/S0263034613000700 Published online by Cambridge University Press

quasi-stationary approximation:

$$\frac{dx_{ks}}{dt} = -x_{ks}\left(\sum_{s'} R_{ks\to k-1,s'} + \sum_{s'} I_{ks\to k+1,s'} + \sum_{s'} \alpha_{ks\to ks'}\right) + \sum_{s'} x_{k+1,s'} R_{k+1,s'\to k,s} + \sum_{s'} x_{k-1,s'} I_{k-1,s'\to k,s} + \sum_{s'} x_{ks'} \alpha_{ks'\to ks} = 0. \quad (15)$$

In Eq. (15) the rate of recombination from the ion state ks to the state $k-1$, s' is given by

$$R_{ks\to k-1,s'} = \alpha^{ir}(ks \to k-1, s') + \alpha^{phr}(ks \to k-1, s') + \alpha^{dc}(ks \to k-1, s'), \quad (16)$$

where $\alpha^{ir}(ks \to k-1, s')$, $\alpha^{phr}(ks \to k-1, s')$, and $\alpha^{dc}(ks \to k-1, s')$ are the rates of three-body recombination, photo-recombination and dielectronic capture, respectively. The rate of ionization from ks to $k+1$, s' state is given by

$$I_{ks\to k+1,s'} = \alpha^{ii}(ks \to k+1, s') + \alpha^{phi}(ks \to k+1, s') + \alpha^{ai}(ks \to k+1, s'), \quad (17)$$

where $\alpha^{ii}(ks \to k+1, s')$, $\alpha^{phi}(ks \to k+1, s')$, and $\alpha^{ai}(ks \to k+1, s')$ are the rates of impact ionization, photo-ionization and auto-ionization, respectively. The rates of transitions from ks to ks' without a change of ionization stage are written as follows

$$\alpha_{ks\to ks'} = \begin{cases} \alpha^{ex}(ks \to ks') + \alpha^{abs}(ks \to ks'), & \text{if } E_{ks} < E_{ks'}, \\ \alpha^{dex}(ks \to ks') + \alpha^{em}(ks \to ks'), & \text{if } E_{ks} > E_{ks'}, \end{cases} \quad (18)$$

where E_{ks} is the energy of ion state ks, $\alpha^{ex}(ks \to ks')$ and $\alpha^{dex}(ks \to ks')$ are the rates of excitation and de-excitation by electron impact, and $\alpha^{abs}(ks \to ks')$, $\alpha^{em}(ks \to ks')$ are the rates of radiative excitation (absorption) and radiative emission, respectively. For calculation of these rates the Regemorter, Lotz and Kramers approximations are used (Nikiforov *et al.*, 2005; Sobel'man *et al.*, 1995).

The number of ion states that must be taken into account can be very large. To reduce the system of kinetic equations we apply a radiative unresolved spectra atomic model (RUSAM) (Kim *et al.*, 2012; Novikov *et al.*, 2010). Knowing the concentrations x_{ks} the tables of spectral absorption coefficients and emissivities are obtained with the code THERMOS (Nikiforov *et al.*, 2005).

The concentrations x_{ks} are defined by the radiation field U_ω through the rates of the radiation processes. The photo-ionization of an electron with quantum numbers $n\ell$ (n is the principal quantum number, ℓ is the orbital quantum number) in Kramers approximation for Q_{ks}-configuration with occupation numbers $N^{ks}_{n\ell}$ has the form:

$$\alpha^{phi}_{n\ell}(ks \to k+1, s') = N^{ks}_{n\ell} u_{n\ell} \int_{\varepsilon_{ks;k+1,s'}/\theta}^{\infty} W(\xi)\xi^{-1} d\xi, \quad (19)$$

where

$$u_{n\ell} = 4.45\times 10^{10} Z_k \frac{|\varepsilon_{ks;k+1,s'}|^{3/2}}{2n^2},$$

$\varepsilon_{ks;k+1,s'} = E_{ks} - E_{k+1,s'}$ is the photo-ionization threshold in atomic units, Z_k is the effective charge, θ is the temperature in atomic units, $W(\xi) = C_\xi U_\omega/\omega^3$ is the radiation energy density in dimensionless units, C_ξ is the dimension factor. For instance, for Planck's radiation field $W(\xi) = [\exp(\xi) - 1]^{-1}$. The photo-recombination rate to the level $n\ell$ in configuration Q_{ks} with occupation numbers $N^{ks}_{n\ell}$ is given by

$$\alpha^{phr}_{n\ell}(k+1, s' \to ks) = C_{n\ell} u_{n\ell} N^{ks}_{n\ell} \times \int_{\varepsilon_{ks;k+1,s'}/\theta}^{\infty} \frac{1 + W(\xi)}{\xi \exp(\xi)} d\xi, \quad (20)$$

where

$$C_{n\ell} = 0.704 \frac{N_e}{N_A} \frac{g_{ks}}{g_{k+1,s'}} \frac{\exp(\varepsilon_{ks;k+1,s'}/\theta)}{\theta^{3/2}},$$

N_A is the Avogadro constant, N_e is the electron density, g_{ks} is the statistical weight for the state ks. For given photon energy intervals $[\omega_i, \omega_{i+1}]$ ($i = 1, N_g$), absorption in lines is defined by

$$\alpha^{abs}_{ks,ks'} = 3.2\times 10^{10} \sum_{i=1}^{N_g} \frac{\overline{gf}_i(ks, ks')}{g_{ks}} \overline{\omega_i}^2(ks, ks') \times W\left(\frac{\overline{\omega_i}(ks, ks')}{\theta}\right), \quad (21)$$

where $\overline{\omega_i}(ks, ks')$ is the center of line group, and $\overline{gf}_i(ks, ks')$ is the oscillator strength averaged over interval $[\omega_i, \omega_{i+1}]$. The line emission rate is given by

$$\alpha^{em}_{ks',ks} = 3.2\times 10^{10} \sum_{i=1}^{N_g} \frac{\overline{gf}_i(ks, ks')}{g_{ks'}} \overline{\omega_i}^2(ks, ks') \times \left[1 + W\left(\frac{\overline{\omega_i}(ks, ks')}{\theta}\right)\right]. \quad (22)$$

Using RUSAM method the absorption coefficient in cm^{-1} for a photon with energy ω in the spectral interval

https://doi.org/10.1017/S0263034613000700 Published online by Cambridge University Press

$[\omega_i, \omega_{i+1}]$ can be written in the form:

$$\kappa_i = \rho\frac{N_A}{A}\left[1-\exp\left(-\omega_i^{\mathrm{ff}}/\theta\right)\right]\left\{\sum_{ks} x_{ks}\sum_{ks'}\sigma_i^{\mathrm{bb}}(ks, ks') + \sum_{ks} x_{ks}\sum_{k+1,s'}\sigma_{ks;k+1,s'}^{\mathrm{bf}}(\omega_i^{\mathrm{bf}}) + \sigma^{\mathrm{ff}}(\omega_i^{\mathrm{ff}})\right\}. \quad (23)$$

The emissivity in TW/(cm$^3\times$ *e*V $\times$ steradian) is written as follows:

$$j_i = \rho\frac{N_A}{A}\frac{1}{C_W}\left[\frac{\overline{\omega_i}^3\,(ks, ks')}{4\pi^3}\alpha^2\right]\left\{\sum_{ks'} x_{ks'}\sum_{ks}\sigma_i^{\mathrm{bb}}(ks', ks) + \sum_{k+1,s'} x_{k+1,s'}\sum_{k,s}\sigma_{k+1,s';ks}^{\mathrm{fb}}(\omega_i^{\mathrm{bf}}) + \exp\left(-\omega_i^{\mathrm{ff}}/\theta\right)\sigma^{\mathrm{ff}}(\omega_i^{\mathrm{ff}})\right\}. \quad (24)$$

Here A is the atomic weight, $C_W = 4.23\times10^{-3}$, $\omega_i^{\mathrm{ff}} = 0.5(\omega_{i+1}+\omega_i)$ is the center of interval,

$$\omega_i^{\mathrm{bf}} = \begin{cases} 0.5(\omega_{i+1}+\omega_i), & \text{if } \varepsilon_{ks;k+1,s'} < \omega_i, \\ \varepsilon_{ks;k+1,s'}, & \text{if } \omega_i < \varepsilon_{ks;k+1,s'} \le \omega_{i+1}. \end{cases}$$

The absorption cross-section in spectral lines can be written in the form:

$$\sigma_i^{\mathrm{bb}}(ks, ks') = 2\pi^2\alpha a_0^2\frac{1}{\omega_{i+1}-\omega_i}\frac{\overline{gf}_i(ks, ks')}{g_{ks}}, \quad (25)$$

and the corresponding emission cross-section is given by

$$\sigma_i^{\mathrm{bb}}(ks', ks) = 2\pi^2\alpha a_0^2\frac{1}{\omega_{i+1}-\omega_i}\frac{\overline{gf}_i(ks, ks')}{g_{ks'}}, \quad (26)$$

where $\alpha \approx 1/137$, $a_0 \approx 5.29\times10^{-9}$ cm is the Bohr radius. For the photo-ionization cross-section, we use the simple Kramers approximation:

$$\sigma_{ks;k+1,s'}^{\mathrm{bf}}(\omega) = \frac{64\pi\alpha a_0^2}{3\sqrt{6}}Z_k\frac{\varepsilon_{ks;k+1,s'}^{3/2}}{\omega^3}\times\frac{N_{n\ell}^{ks}}{2n^2}\left[1-n(\varepsilon_{ks;k+1,s'}-\omega)\right],\ \text{if } \omega > \varepsilon_{ks;k+1,s'}, \quad (27)$$

$\sigma_{ks;k+1,\ s'}^{\mathrm{bf}}(\omega) = 0$, if $\omega < \varepsilon_{ks;k+1,s'}$, with photo-ionization threshold $\varepsilon_{ks;k+1,s'} = E_{ks} - E_{k+1,\ s'}$ in atomic units. The photo-recombination cross-section to the state ks has the form:

$$\sigma_{k+1,s';ks}^{\mathrm{fb}}(\omega) = \frac{64\pi\alpha a_0^2}{3\sqrt{6}}Z_k\frac{\varepsilon_{ks;k+1,s'}^{3/2}}{\omega^3}\times\frac{2(2\ell+1)-N_{n\ell}^{k+1,s'}}{2n^2}n(\varepsilon_{ks;k+1,s'}-\omega),\ \text{if}\omega > \varepsilon_{ks;k+1,s'}, \quad (28)$$

$\sigma_{k+1,s';ks}^{\mathrm{fb}}(\omega) = 0$, if $\omega < \varepsilon_{ks;k+1,s'}$. Here $n(\varepsilon) = [1+\exp\left(-\frac{\varepsilon+\mu}{\theta}\right)]^{-1}$ is the free electrons distribution function μ is the chemical potential. The bremsstrahlung cross section is calculated in the Born-Elwert approximation

$$\sigma^{\mathrm{ff}}(\omega) = 2.384\times10^{6\frac{\rho Z_0^2\theta}{A\omega^3}}\int_{\varepsilon_0}^{\infty} n(\varepsilon)\left[1-n(\varepsilon')\right]g(\varepsilon', \varepsilon)\mathrm{d}\varepsilon, \quad (29)$$

where $\varepsilon' = \varepsilon + \omega$ and

$$g(\varepsilon', \varepsilon) = \frac{\sqrt{3}}{\pi}\sqrt{\frac{\varepsilon'}{\varepsilon}}\ln\left(\frac{\sqrt{\varepsilon'}+\sqrt{\varepsilon}}{\sqrt{\varepsilon'}-\sqrt{\varepsilon}}\right)\frac{1-\exp\left[-2\pi Z_0/\sqrt{2\varepsilon'}\right]}{1-\exp\left[-2\pi Z_0/\sqrt{2\varepsilon}\right]}.$$

The radiation field and level kinetics are accounted self-consistently by using an approach with interpolation between pre-calculated tables of spectral parameters.

Spectral absorption coefficients K_ω and emissivities j_ω are calculated using a collisional-radiative equilibrium model in quasi-stationary approximation for an optically-transparent plasma (radiation field $U_\omega = 0$) and for plasma in thermodynamic equilibrium with Planck's radiation field ($U_\omega = U_\omega^P$) (Novikov & Solomyannaya, 1998):

$$U_\omega^P = \frac{60}{c\pi^4}\sigma\frac{\omega^3}{\exp(\omega/T)-1}, \quad (30)$$

where $\sigma = 1.028\times10^{-7}$ TW/cm^2/eV^4 is the Stefan–Boltzmann constant (here ω and T are measured in eV, $c \approx 3\times10^{10}$ cm/s). It should be noted that the transparent plasma approximation comes to thermodynamic equilibrium at high densities (due to collisional processes) and gives the coronal equilibrium at low densities.

The ratio between calculated radiation field and Planck's radiation field is used as an interpolation parameter:

$$\zeta(z, t) = \frac{\int_0^\infty U_\omega(z, t)\mathrm{d}\omega}{\int_0^\infty U_\omega^P\mathrm{d}\omega}. \quad (31)$$

Applying parameter ζ, the absorption coefficients K_ω and emissivities j_ω are calculated as follows:

$$\kappa_\omega = (1-\zeta)\kappa_\omega^{(U_\omega=0)} + \zeta\kappa_\omega^{(U_\omega=U_\omega^P)},$$
$$j_\omega = (1-\zeta)j_\omega^{(U_\omega=0)} + \zeta j_\omega^{(U_\omega=U_\omega^P)}, \quad (32)$$

where $\kappa_\omega^{(U_\omega=0)}, j_\omega^{(U_\omega=0)}$ are the absorption coefficients and emissivities for optically-transparent plasma, and $\kappa_\omega^{(U_\omega=U_\omega^P)}, j_\omega^{(U_\omega=U_\omega^P)}$ are the absorption coefficients and emissivities for plasma in thermodynamic equilibrium.

After that two types of mean group absorption coefficients are calculated by using Rosseland $R(\xi) = \xi^4\exp(-\xi)/[1-\exp(-\xi)]^2$, and Planck $P(\xi) = \xi^3\exp(-\xi)/[1-\exp(-\xi)]$

https://doi.org/10.1017/S0263034613000700 Published online by Cambridge University Press

weight functions:

$$\kappa^R_{g_i} = \frac{\int_{\xi_i}^{\xi_{i+1}} R(\xi)\mathrm{d}\xi}{\int_{\xi_i}^{\xi_{i+1}} R(\xi)/\kappa_\omega \mathrm{d}\xi}, \kappa^P_{g_i} = \frac{\int_{\xi_i}^{\xi_{i+1}} P(\xi)\kappa_\omega \mathrm{d}\xi}{\int_{\xi_i}^{\xi_{i+1}} P(\xi)\mathrm{d}\xi}. \quad (33)$$

The group emission coefficient is calculated as follows:

$$j_{g_i} = \frac{\int_{\xi_i}^{\xi_{i+1}} j_\omega \mathrm{d}\xi}{\xi_{i+1} - \xi_i}. \quad (34)$$

Here $\xi = \omega/T$, and the index g_i denotes the heat radiation frequency range $\omega_i \le \omega \le \omega_{i+1}$ for $i = 1, \ldots N_g$, where N_g is the number of groups ($N_g = 96$ in the presented below results).

Now, the system (12)–(14) can be written in a group approximation and transformed to the diffusion equation with appropriate boundary conditions so that

$$\frac{\partial}{\partial z}\left(-\frac{c}{3\kappa^R_{g_i}}\frac{\partial U_{g_i}}{\partial z}\right) = 4\pi j_{g_i} - \kappa^P_{g_i} c U_{g_i}. \quad (35)$$

The tables of coefficients for CH_2 are obtained by applying a mixing procedure of the tables for pure elements C and H. At given temperature the equality of chemical potentials (electron densities) of the mix components is suggested (Nikiforov *et al.*, 2005).

RESULTS AND DISCUSSION

Previously (Povarnitsyn *et al.*, 2012*a*), we have investigated the undesirable action of the long nanosecond prepulse on the target and the possible solution for the contrast improvement by means of a thin metal film. Initially, the transmission of the cold film is zero because of supercritical electron density and the prepulse does not reach the main target. Then, the expansion of the heated film starts resulting in the increase of energy absorption up to 100%, high temperatures and flat density profile ofthe plasma in front of the film. Eventually, the electron density in the film plasma drops below the critical value. Such undercritical plasma is now transparent for the laser beam. For different initial thicknesses of the film we observe various moments of transparency, and thus one can adjust the thickness so that the film becomes transparent at the moment of the main pulse arrival. In our numerical experiment, the laser pulse time profile is used in the form

$$I(t) = I_{\max}\left\{C_{\mathrm{ns}} + C_{\mathrm{ps}} \exp\left[-\ln(16)t^2/\tau_1^2\right] + \exp\left[-\ln(16)t^2/\tau_0^2\right]\right\}$$

with $I_{\max} = 10^{19}$ W/cm^2, $C_{\mathrm{ns}} = 10^{-6}$, $C_{\mathrm{ps}} = 10^{-4}$, $\tau_0 = 0.5$ ps, $\tau_1 = 20$ ps and $-2000 \le t \le 20$ ps. This profile is typical for petawatt laser facilities (Bagnoud *et al.*, 2010), and the prepulse intensity level is of the order of 10^{13} W/cm^2 that is sufficient for ionization of dielectrics during several picoseconds (Du *et al.*, 1994; Stuart *et al.*, 1995). Thus, we can use not only the metal Al film for target shielding but also a CH_2 one. For the CH_2 film, the Thomas–Fermi model (Fromy *et al.*, 1996) gives the mean ion charge $\langle Z \rangle = 1.12$ at normal conditions that corresponds to preionized supercritical state.

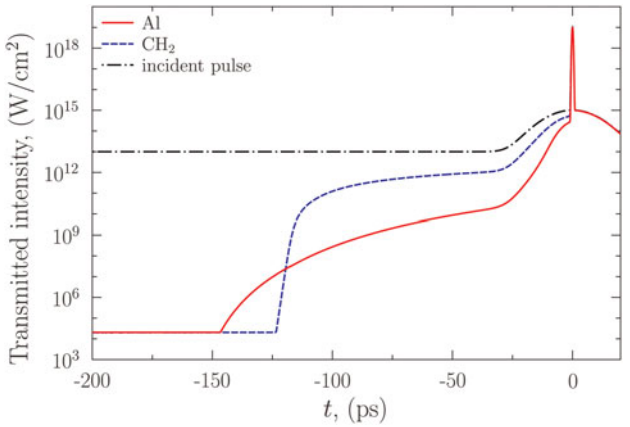

Fig. 3. (Color online) Intensity transmitted through the films. Solid (red) curve — 400 nm Al film; dashed (blue) curve — 2250 nm CH_2 film; dashed-and-dot (black) curve — incident intensity of the laser pulse.

The "optimal" thicknesses of Al and CH_2 films are calculated in a set of simulations to be 400 and 2250 nm, respectively. As one can see in Figure 3 such films can diminish the level of transmitted intensity during the prepulse action while the main subpicosecond pulse can easily pass through the film plasma.

Nevertheless, as was previously shown the laser energy transformation into the soft X-ray radiation results in strong emission of the film plasma that causes the preheating of the main target. In Figure 4, the ratio of radiation flux integrated over the spectrum from 0 to 10 keV to the incident intensity, $S(t)/I(t)$, is presented. The ratio can reach as much as 7% on the back side of the Al film (at $t \approx -700$ ps) and up to 11% on the front side for the Al film (at moment $t \approx -1400$ ps). As it is discussed below, this value is

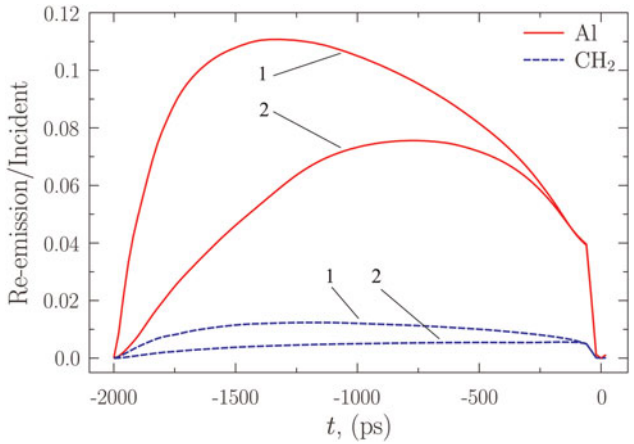

Fig. 4. (Color online) Thermal radiation flux in front (1) and back (2) directions for Al and CH_2 films.

https://doi.org/10.1017/S0263034613000700 Published online by Cambridge University Press

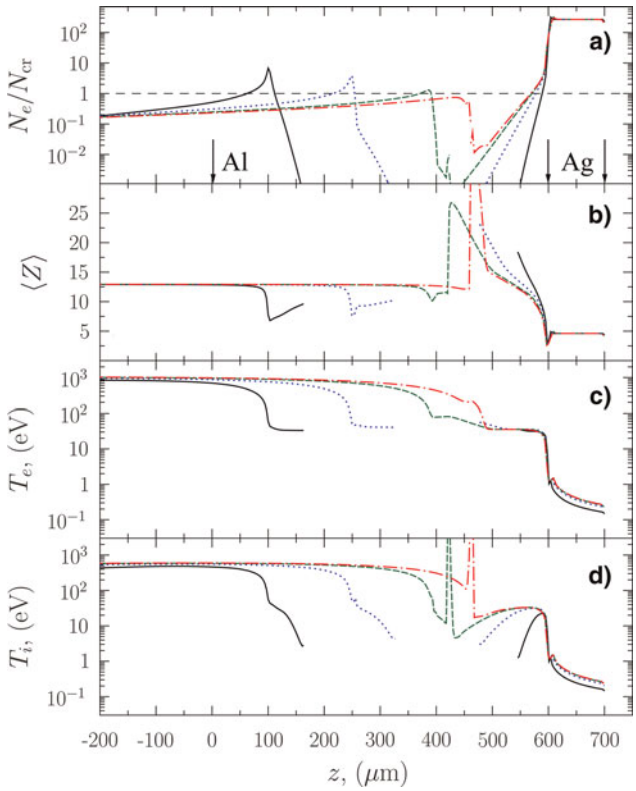

Fig. 5. (Color online) Evolution of the main parameters in the shielding Al film (400 nm) and the target of Ag (100 μm). Electron density normalized to the critical one — (a); mean charge of ions — (b); electron temperature — (c); ion temperature — (d). Instants: solid (black) curve — −1000 ps; dotted (blue) curve — −500 ps; dashed (green) curve — −200 ps; dash-and-dot (red) curve — −100 ps. Initial positions of Al film and Ag target are presented in panel (a).

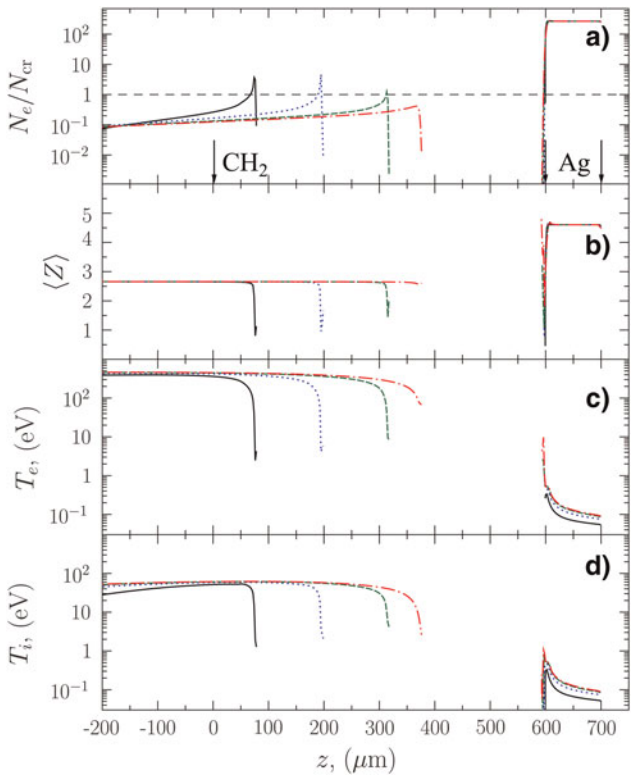

Fig. 6. (Color online) The same, as in Figure 5 but for CH_2 (2250 nm) shielding film.

sufficient to produce a noticeable main target preheating, expansion, and ionization. Initial positions of the Al film and Ag bulk target are shown in Figure 5a. The gap between the film and the target is 600 μm. The target surface rarefaction is already noticeable by the moment $t = -1000$ ps. The target plasma interacts with the film plasma at $t \approx -200$ ps and $z \approx 425$ μm (peaks in panels a, b, and d). The characteristic temperature in the film plasma is about 900 eV. It is clearly seen in Figure 5a the subsequent decrease in electron density from a supercritical value (at $t = -1000$, -500, -200 ps) to an undercritical one at $t = -100$ ps. The ionization degree in Ag plasma reaches ≈25 and the extent of plasma is about 150 μm. At the same time the temperature of the bulk target is not larger than 1 eV, but the presence of extending plasma with a near-critical density can change the interaction of the main pulse with the target. Moreover, our 1D simulation can overestimate the temperature in the film plasma due to the laser spot size limitation and 3D nature of the plasma spread in experiment.

In contrast to the situation considered, usage of the CH_2 film gives approximately an order less intensity of the radiation flux (see Fig. 4), and as a result the relatively low preheating of the target is observed. During the prepulse action, even by the moment $t = -100$ ps the target rarefaction is negligible, see Figure 6a. The temperature of the target is of the order of 1 eV while the film substance is fully ionized by the moment $t = -100$ ps and the temperatures of electrons and ions are 400 and 40 eV, respectively.

The model of radiation transport gives the spectral distribution of photon energies. A comparison of the spectra of Al and CH_2 is presented in Figure 7 and shows that aluminum plasma has a greater emissivity in the range from 0 to 900 eV. The maximum emission is produced by dense

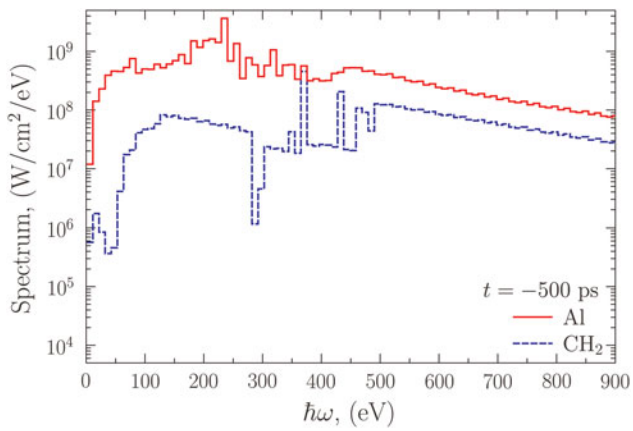

Fig. 7. (Color online) Spectrum of re-emission from the back side of the films for moment $t = -500$ ps: Al — solid (red); CH_2 — dashed (blue).

https://doi.org/10.1017/S0263034613000700 Published online by Cambridge University Press

plasma of Al in the range 200–300 eV, while for the CH_2 plasma the emission maximum is in the range 350–450 eV. The K_α emission lines of Al are located at about 2 keV and do not give a noticeable contribution to the radiation energy flux. Thus, the application of thin films composed of light elements (CH, CH_2, ect.) might be effective in the contrast modification and improvement.

CONCLUSION

For the investigation of the dynamics of thin Al and CH_2 films as well as the Ag bulk target irradiated by long nanosecond prepulses we have used the two-temperature single-fluid radiation hydrodynamic model. This model describes the laser energy absorption, electron-ion coupling and two-temperature effects, radiation transport, thermodynamic properties of materials. Using the model we have studied the action of a nanosecond prepulse on Al and CH_2 films. The balance between the incident laser intensity, transmitted laser intensity and radiation flux is investigated in numerical experiment. The fraction of the laser energy transmitted through the film is determined together with the estimation of emitted thermal radiation flux.

We have found out that there is an "optimal" film thickness that can totally diminish the prepulse energy transmittance and become transparent by the moment of the main high-intensity subpicosecond laser pulse arrival. At the same time the re-emission of the prepulse energy by the shielding film can be significant for Al films producing an undesirable preheating and rarefaction of the main target placed behind the film. Fortunately, for a CH_2 film it is observed a one-order less re-emission flux which does not produce an essential target disturbance. Thus, films composed of light elements can be effective in cutting of nanosecond low-intensity prepulses.

ACKNOWLEDGMENTS

The research was sponsored by the Russian Foundation for Basic Research (Project Nos. 13-08-01179, 11-02-91058, 11-08-01225, 13-08-12248 and 13-02-91057) and the Council of the President of the Russian Federation for Support of Young Russian Scientists and Leading Scientific Schools (Grant No. NSh-7241.2012.2).

REFERENCES

Apfelbaum, E.M. (2011). Calculation of electronic transport coefficients of Ag and Au plasma. *Phys. Rev. E* **84**, 066403.

Bagnoud, V., Aurand, B., Blazevic, A., Borneis, S., Bruske, C., Ecker, B., Eisenbarth, U., Fils, J., Frank, A., Gaul, E., Goette, S., Haefner, C., Hahn, T., Harres, K., Heuck, H.-M., Hochhaus, D., Hoffmann, D., Javorkova, D., Kluge, H.-J., Kuehl, T., Kunzer, S., Kreutz, M., Merz-Mantwill, T., Neumayer, P., Onkels, E., Reemts, D., Rosmej, O., Roth, M., Stoehlker, T., Tauschwitz, A., Zielbauer, B., Zimmer, D. & Witte, K. (2010). Commissioning and early experiments of the PHELIX facility. *Appl. Phys. B: Lasers Opt.* **100**, 137–150.

Carroll, D.C., Tresca, O., Prasad, R., Romagnani, L., Foster, P.S., Gallegos, P., Ter-Avetisyan, S., Green, J.S., Streeter, M.J.V., Dover, N., Palmer, C.A.J., Brenner, C.M., Cameron, F.H., Quinn, K.E., Schreiber, J., Robinson, A.P.L., Baeva, T., Quinn, M.N., Yuan, X.H., Najmudin, Z., Zepf, M., Neely, D., Borghesi, M. & McKenna, P. (2010). Carbon ion acceleration from thin foil targets irradiated by ultrahigh-contrast, ultraintense laser pulses. *New J. Phys.* **12**, 045020.

Ditmire, T., Bless, S., Dyer, G., Edens, A., Grigsby, W., Hays, G., Madison, K., Maltsev, A., Colvin, J., Edwards, M.J., Lee, R.W., Patel, P., Price, D., Remington, B.A., Sheppherd, R., Wootton, A., Zweiback, J., Liang, E. & Kielty, K.A. (2004). Overview of future directions in high energy-density and high-field science using ultra-intense lasers. *Radiat. Phys. Chem.* **70**, 535–552.

Doumy, G., Quéré, F., Gobert, O., Perdrix, M., Martin, P., Audebert, P., Gauthier, J.C., Geindre, J.-P. & Wittmann, T. (2004). Complete characterization of a plasma mirror for the production of high-contrast ultraintense laser pulses. *Phys. Rev. E* **69**, 026402.

Du, D., Liu, X., Korn, G., Squier, J. & Mourou, G. (1994). Laser-induced breakdown by impact ionization in SiO_2 with pulse widths from 7 ns to 150 fs. *Appl. Phys. Lett.* **64**, 3071–3073.

Fromy, P., Deutsch, C. & Maynard, G. (1996). Thomas–Fermi-like and average atom models for dense and hot matter. *Phys. Plasmas* **3**, 714.

Khishchenko, K.V. (2008). Equation of state and phase diagram of tin at high pressures. *J. Phys.: Conf. Ser.* **121**, 022025.

Khishchenko, K.V., Tkachenko, S.I., Levashov, P.R., Lomonosov, I.V. & Vorob'ev, V.S. (2002). Metastable states of liquid tungsten under subsecond wire explosion. *Int. J. Thermophys.* **23**, 1359.

Kim, D.A., Novikov, V.G., Dolgoleva, G.V., Koshelev, K.N. & Solomyannaya, A.D. (2012). EUV-source modeling with account of detailed level kinetics included in-line into gasdynamic calculations. Technical Report **51**. URL: http://library.keldysh.ru/preprint.asp?id=2012-51

Kitagawa, Y., Fujita, H., Kodama, R., Yoshida, H., Matsuo, S., Jitsuno, T., Kawasaki, T., Kitamura, H., Kanabe, T., Sakabe, S., Shigemori, K., Miyanaga, N. & Izawa, Y. (2004). Prepulse-free petawatt laser for a fast ignitor. *IEEE J. Quan. Electron.* **40**, 281–293.

Levashov, P.R. & Khishchenko, K.V. (2007). Tabular multiphase equations of state for metals and their applications. *AIP Conf. Proc.* **955**, 59–62.

Lin, Z., Zhigilei, L.V. & Celli, V. (2008). Electron-phonon coupling and electron heat capacity of metals under conditions of strong electron-phonon nonequilibrium. *Phys. Rev. B* **77**, 075133.

McKenna, P., Lindau, F., Lundh, O., Neely, D., Persson, A. & Wahlström, C.-G. (2006). High-intensity laser-driven proton acceleration: influence of pulse contrast. *Philosoph. Trans. Royal Soci. A* **364**, 711–723.

Nikiforov, A.F., Novikov, V.G. & Uvarov, V.B. (2005). *Quantum-Statistical Models of Hot Dense Matter: Methods for Computation Opacity and Equation of State*. Basel: Birkhäusen Verlag.

Novikov, V.G., Koshelev, K.N. & Solomyannaya, A.D. (2010). Radiative unresolved spectra atomic model, *in* V.E. Fortov et al., eds, 'Physics of Extreme States of Matter — 2010', IPCP, Chernogolovka, pp. 21–24.

Novikov, V.G. & Solomyannaya, A.D. (1998). Spectral characteristics of plasma consistent with radiation. *High Temp.* **36**, 858–864.

Oreshkin, V.I., Baksht, R.B., Ratakhin, N.A., Shishlov, A.V., Khishchenko, K.V., Levashov, P. & Beilis, I.I. (2004). The thermal instabilities on electrical explosion of metal wires. *Phys. Plasmas* **11**, 4771.

Ovchinnikov, A.V., Kostenko, O.F., Chefonov, O.V., Rosmej, O.N., Andreev, N.E., Agranat, M.B., Duan, J.L., Liu, J. & Fortov, V.E. (2011). Characteristic X-rays generation under the action of femtosecond laser pulses on nano-structured targets. *Laser Parti. Beams* **29**, 249–254.

Povarnitsyn, M.E., Andreev, N.E., Levashov, P.R., Khishchenko, K.V. & Rosmej, O.N. (2012*a*). Dynamics of thin metal foils irradiated by moderate-contrast high-intensity laser beams. *Phys. Plasmas* **19**, 023110.

Povarnitsyn, M.E., Andreev, N.E., Apfelbaum, E.M., Itina, T.E., Khishchenko, K.V., Kostenko, O.F., Levashov, P.R. & Veysman, M.E. (2012*b*). A wide-range model for simulation of pump-probe experiments with metals. *Appl. Surf. Sci.* **258**, 9480–9483.

Shemyakin, O.P., Levashov, P.R., Obruchkova, L.R. & Khishchenko, K.V. (2010). Thermal contribution to thermodynamic functions in the Thomas–Fermi model. *J. Phys. A: Math. Theor.* **43**, 335003.

Sobel'man, I.I., Vainshtein, L.A. & Youkov, E.A. (1995). *Excitation of Atoms and Broadening of Spectral Lines, translated from the Russian*. Moscow: Springer-Verlag.

Spitzer, L. & Härm, R. (1953). Transport phenomena in a completely ionized gas. *Phys. Rev.* **89**, 977–981.

Stehlé, C., González, M., Kozlova, M., Rus, B., Mocek, T., Acef, O., Colombier, J.P., Lanz, T., Champion, N., Jakubczak, K., Polan, J., Barroso, P., Bauduin, D., Audit, E., Dostal, J. & Stupka, M. (2010). Experimental study of radiative shocks at PALS facility. *Laser Parti. Beams* **28**, 253–261.

Stuart, B.C., Feit, M.D., Rubenchik, A.M., Shore, B.W. & Perry, M.D. (1995). Laser-induced damage in dielectrics with nanosecond to subpicosecond pulses. *Phys. Rev. Lett.* **74**, 2248–2251.

Veysman, M.E., Agranat, M.B., Andreev, N.E., Ashitkov, S.I., Fortov, V.E., Khishchenko, K.V., Kostenko, O.F., Levashov, P.R., Ovchinnikov, A.V. & Sitnikov, D.S. (2008). Femtosecond optical diagnostics and hydrodynamic simulation of Ag plasma created by laser irradiation of a solid target. *J. Phys. B: At., Molec. Opti. Phys.* **41**, 125704.

Zastrau, U., Audebert, P., Bernshtam, V., Brambrink, E., Kämpfer, T., Kroupp, E., Loetzsch, R., Maron, Y., Ralchenko, Y., Reinholz, H., Röpke, G., Sengebusch, A., Stambulchik, E., Uschmann, I., Weingarten, L. & Förster, E. (2010). Temperature and $K\alpha$-yield radial distributions in laser-produced solid-density plasmas imaged with ultrahigh-resolution X-ray spectroscopy. *Phys. Rev. E* **81**, 026406.